PHOTONICS Research

Silicon-based four-mode division multiplexing for chip-scale optical data transmission in the 2 μm waveband

Shuang Zheng,[1,†] Meng Huang,[1,†] Xiaoping Cao,[1] Lulu Wang,[1] Zhengsen Ruan,[1] Li Shen,[1,2] and Jian Wang[1,3]

[1]Wuhan National Laboratory for Optoelectronics, School of Optical and Electronic Information, Huazhong University of Science and Technology, Wuhan 430074, China
[2]e-mail: lishen@hust.edu.cn
[3]e-mail: jwang@hust.edu.cn

Received 22 March 2019; revised 25 June 2019; accepted 8 July 2019; posted 9 July 2019 (Doc. ID 363095); published 14 August 2019

Based on a silicon platform, we design and fabricate a four-mode division (de)multiplexer for chip-scale optical data transmission in the 2 μm waveband for the first time, to the best of our knowledge. The (de)multiplexer is composed of three tapered directional couplers for both mode multiplexing and demultiplexing processes. In the experiment, the average crosstalk for four channels is measured to be less than −18 dB over a wide wavelength range (70 nm) from 1950 to 2020 nm, and the insertion losses are also assessed. Moreover, we further demonstrate stable 5 Gbit/s direct modulation data transmission through the fabricated silicon photonic devices with non-return-to-zero on–off keying signals. The experimental results show clear eye diagrams, and the penalties at a bit error rate of 3.8×10^{-3} are all less than 2.5 dB after on-chip data transmission. The obtained results indicate that the presented silicon four-mode division multiplexer in the mid-infrared wavelength band might be a promising candidate facilitating chip-scale high-speed optical interconnects.

https://doi.org/10.1364/PRJ.7.001030

1. INTRODUCTION

The mid-infrared (MIR) spectral region used for biomedical and sensing applications is of great importance, because most molecules display stronger fundamental vibrational absorptions in this region [1–3]. Not only that, the pursuit of high-capacity optical communications in the MIR spectral region has intensified in recent years. The realization of a low-loss hollow core photonic bandgap fiber (HC-PBGF) waveband offers a great opportunity to realize a wide and low-loss 2 μm transmission window [4]. Furthermore, thulium-doped fiber amplifiers (TDFAs) provide an exceptionally wide (100 nm) bandwidth in this wavelength range, and thus long-distance communication in the 2 μm transmission window is considered to be feasible [5]. From then on, several high-speed and high-capacity optical communication systems have been demonstrated experimentally by using the proposed HC-PBGF or other fibers [6–8]. 100 Gbit/s wavelength-division multiplexing (WDM) transmission in the 2 μm waveband was successfully demonstrated over 1.15 km of low-loss HC-PBGF and over 1 km of solid core fiber (SCF) [6]. After that, an externally modulated 4×10 Gbit/s non-return-to-zero (NRZ) on–off keying (OOK) WDM signal transmitted through 1.15 km of low-loss HC-PBGF, employing an InP-based Mach–Zehnder modulator (MZM) for the first time [7], to the best of our knowledge. Recently, 80 Gbit/s data transmission using the direct-detection optical filter bank multicarrier (FBMC) modulation technique is achieved, which is the highest single-channel bit rate through a 100-m-long SCF designed for single-mode transmission at 2 μm [8].

To reach the potential of WDM and coherent communications in the 2 μm waveband, a suite of active and passive functional integrated components should be designed to improve the performance of the transmission system. As known, the matured complementary metal–oxide–semiconductor (CMOS) technology has been developed for integrated silicon photonics, which has the distinct advantages of small footprint, high density, low loss, and reduced power consumption with improved stability [9–17]. Until now, many key components in 2 μm optical communication systems have been implemented on InP, silicon, and other semiconductor materials systems, such as MIR lasers [18–21], MIR modulators [22–25], and high-speed MIR photodetectors (PDs) [26–29]. Besides, much research on basic passive functional MIR devices has been reported, such as MIR fiber-to-chip grating couplers [30], multimode interferometer (MMI) [31,32], Mach–Zehnder interferometer (MZI) couplers [33], arrayed waveguide grating

(AWG) [34–38], microring resonators (MRRs) [39,40], and polarization control devices [41]. In addition, the mode-division multiplexing (MDM) technique provides another dimension to increase the optical transmission capacity [42–46]. It is believed that the on-chip mode (de)multiplexer at 2 μm has a great potential for chip-scale high-speed optical interconnect applications.

In this paper, we design and fabricate on-chip two-mode and four-mode division multiplexing photonic circuits at the wavelength of 2 μm by using tapered asymmetrical directional couplers. The mode (de)multiplexers and vertical grating coupler are fabricated on a silicon-on-insulator (SOI) platform. In the experiment, the coupling loss of the grating coupler and the average crosstalk of four channels are measured over a wide wavelength range from 1950 to 2020 nm. Moreover, stable data transmission with 5 Gbit/s NRZ-OOK through the fabricated mode (de)multiplexers is further demonstrated. The experimental results including clear eye diagrams and bit error rate (BER) curves are obtained, and the penalties at a BER of 3.8×10^{-3} are less than 2.5 dB for all the channels.

2. CONCEPT AND PRINCIPLE

As shown in Fig. 1, the four-mode division multiplexing structure is composed of a mode multiplexer and a mode demultiplexer, which both have three tapered directional couplers and four input/output ports. Compared to a conventional asymmetrical normal directional coupler, the tapered structure has greater fabrication tolerance and wider working bandwidth [43]. As shown in Fig. 1, inset is the zoom-in view of the tapered asymmetric directional coupler, which parallel-couples a narrow silicon waveguide with width w_1 to a wide tapered waveguide (from w_{2a} to w_{2b} with a center width of w_2) with a coupling length L and gap g, respectively. The adiabatic couplings from the fundamental mode to higher-order modes (TE_0 – TE_1, TE_0 – TE_2, TE_0 – TE_3) rely on the phase matching between the waveguides, i.e., the effective refractive index of the fundamental TE_0 mode of the narrow waveguide equal that of the high-order mode in the wide waveguide at the center wavelength of 2 μm. The conversion process can be described as follows: from input ports, the fundamental mode TE_0 is first used for the excitation of high-order modes via the tapered directional couplers. After a propagation distance, these four modes are then converted back into the fundamental modes for detection by the corresponding asymmetric directional coupler.

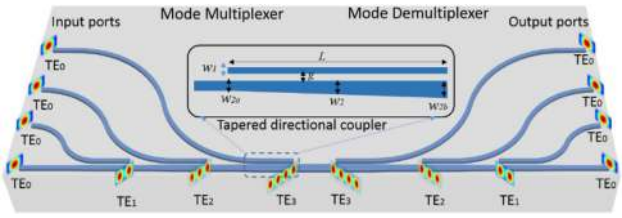

Fig. 1. Schematic structure for four-mode (de)multiplexer on silicon platform. Inset is the zoom-in view of the tapered directional coupler for mode conversion.

3. SIMULATION RESULTS

By using the finite difference eigenmode (FDE) method, we first calculate the dispersion relationship about the mode effective refractive index and width of the silicon waveguide with height $h = 0.22$ μm at the wavelength of 2 μm. As shown in Fig. 2(a), width $w = 0.65$ μm for the TE_0 mode of the narrow waveguide, central width $w = 1.32$ μm for the TE_1 mode, central width $w = 2.02$ μm for the TE_2 mode, and central width $w = 2.705$ μm for the TE_3 mode of the wide waveguide are chosen since their effective indices have almost the same value $n_{\text{eff}} = 2.18$. In order to relax the fabrication limitations, we then design these sloped tapers with $\Delta w = w_{2b} - w_{2a} = 0.1$ μm, as shown in Fig. 2(a). By using the three-dimensional (3D) finite-difference time-domain (FDTD) method, we then simulate the whole transmission process for three high-order modes. In Figs. 2(b)–2(d), it can be observed that the fundamental mode is converted into the desired high-order modes by the asymmetric directional coupler. The mode transmission and crosstalk (less than −18 dB) are calculated and presented in Figs. 2(b)–2(d).

The optimal widths for all the waveguides of the designed four asymmetric directional couplers are summarized, as shown in Table 1. For the asymmetric directional couplers, the width of the narrow waveguide and the gap are chosen to be 0.65 and 0.2 μm, respectively. According to the phase matching condition shown in Fig. 2, we simulate the whole evolution processes and obtain the optimized coupling lengths of 69.8, 91.8, and 94.8 μm for the TE_1, TE_2, and TE_3 modes.

4. EXPERIMENTAL RESULTS AND DISCUSSION

The measured microphotograph of the fabricated four-channel MDM device is shown in Fig. 3(a), which consists of a four-mode multiplexer and demultiplexer. The designed silicon photonic device is fabricated on a standard SOI wafer with a 220-nm-thick top silicon layer and a 2-μm-thick buried oxide (SiO_2) layer. The proposed structure is fabricated by the

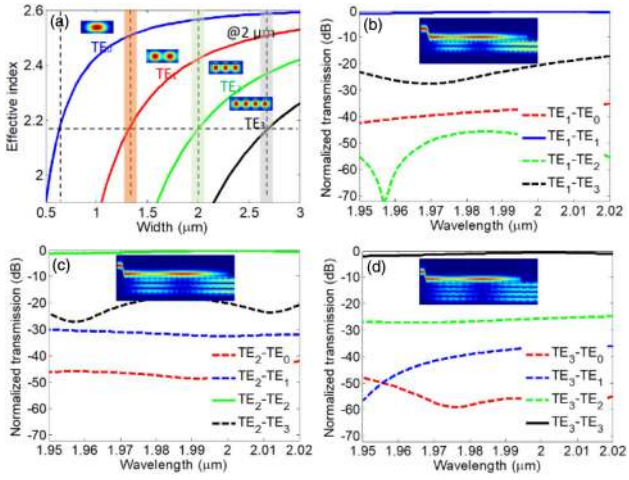

Fig. 2. (a) Simulated effective indices of four multiplexed eigenmodes of a SiO_2-cladding silicon waveguide versus waveguide width w for a waveguide height $h = 220$ nm. (b)–(d) Simulated mode transmission and crosstalk for three high-order modes. Insets are the mode evolution processes.

Table 1. Optimal Geometric Parameters of the Designed 2 μm Mode (De)Multiplexer

	w_1 (μm)	G (μm)	w_2 (μm)	w_{2a} (μm)	w_{2b} (μm)	L (μm)
TE_1	0.65	0.2	1.32	1.27	1.37	69.8
TE_2	0.65	0.2	2.02	1.97	2.07	91.8
TE_3	0.65	0.2	2.705	2.655	2.755	94.8

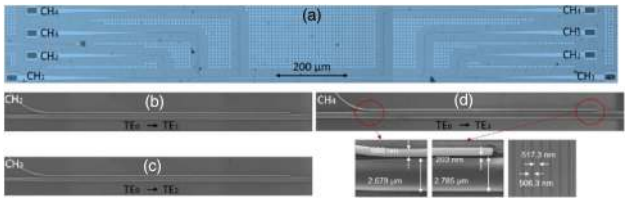

Fig. 3. Optical microscope image and scanning electron microscope (SEM) pictures of the fabricated four-mode division multiplexing device in the 2 μm waveband. (a) The microphotograph of the whole structure. (b)–(d) The details of three tapered directional couplers for (b) TE_1, (c) TE_2, and (d) TE_3 modes. Insets of (d) show the zoom-in details with marked geometric parameters.

248-nm-deep ultraviolet lithography and inductively coupled plasma etching. Waveguide outlines are etched fully down 220 nm to the buried oxide, while the grating couplers are shallow etched down nominally 70 nm. The size of the fabricated device is ∼1.8 mm × 0.23 mm, and the length of four-mode multiplexing is 200 μm. The microscope image in Fig. 3(a) shows the whole view of the device. Details of three asymmetric directional couplers and the vertical grating coupler are shown in Figs. 3(b)–3(d). The width of the narrow waveguide is 660 nm, the wide waveguide is tapered from 2.678 to 2.785 μm, and the coupling gap is 203 nm, as shown in Fig. 3(d). As a comparison, we characterize the performance of the fabricated two-mode (TE_0, TE_1) multiplexing structure first, which has the same structure parameters as shown in Fig. 3(b).

In the experiment, a supercontinuum source (OYSL SC-5-FC) and a long wavelength optical spectrum analyzer (Yokogawa AQ6375B) are used to measure the transmission spectra from the output ports. As shown in Fig. 4(a), the discrepancy between the measured insertion loss of the vertical grating couplers and the simulated coupling efficiency is probably due to an over-etching error that occurred in the fabrication. Most insertion loss of a single straight waveguide comes from the vertical grating coupler, including ∼20 dB coupling loss from the fiber-chip/chip-fiber vertical coupling system for TE polarization around the wavelength of 2 μm. The transmission spectra and the crosstalk of two channels are measured by coupling the broadband optical source into the input ports one by one. By detaching the grating loss and the laser's power fluctuation, the transmission spectra and the crosstalk of two channels are depicted in Figs. 4(b) and 4(c). Obviously, low crosstalk of less than −18 dB between the TE_0 and TE_1 modes can be obtained, owing to the successful mode coupling process.

After that, the four-mode multiplexing device is measured. With the transmission of a straight waveguide as a reference,

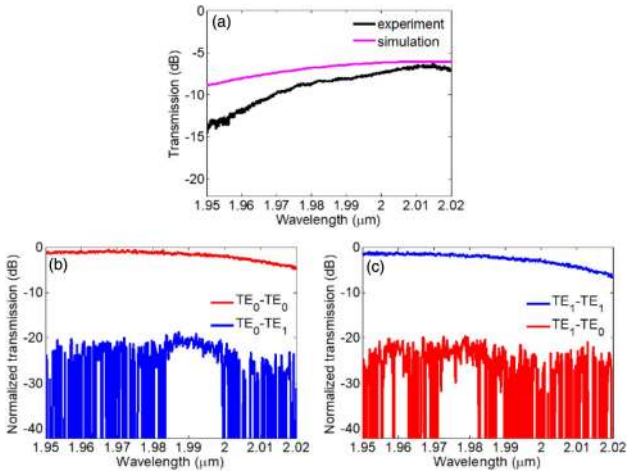

Fig. 4. (a) Measured and simulated transmission spectra of the vertical grating coupler. (b), (c) Measured transmission spectra at two output ports when the TE_0 mode is launched at the input ports of the two-mode multiplexing structure.

the present four-mode (de)multiplexer has an average insertion loss (around 2 μm) of about 1.3, 2.6, 4.8, and 5 dB for the TE_0, TE_1, TE_2, and TE_3 mode channels, respectively. The excess loss is mainly caused by the scattering loss and incomplete mode coupling in the asymmetric directional couplers due to the practical fabrication deviations. The average crosstalk of four channels is less than −18 dB with a wavelength range of ∼70 nm (from 1950 to 2020 nm). Among the measured curves, the curves of four colors (red, blue, green, and black) correspond to the detected powers of the TE_0, TE_1, TE_2, and TE_3 modes, respectively. As shown in Fig. 5(a), the measured TE_0 mode has a relatively higher power than other three modes. In particular, for the TE_2 and TE_3 modes in Figs. 5(c) and 5(d), the transmission curves tend to descend when coming to a longer wavelength, which is mainly caused by the fabrication deviation. As shown in Fig. 3(d), the widths of the

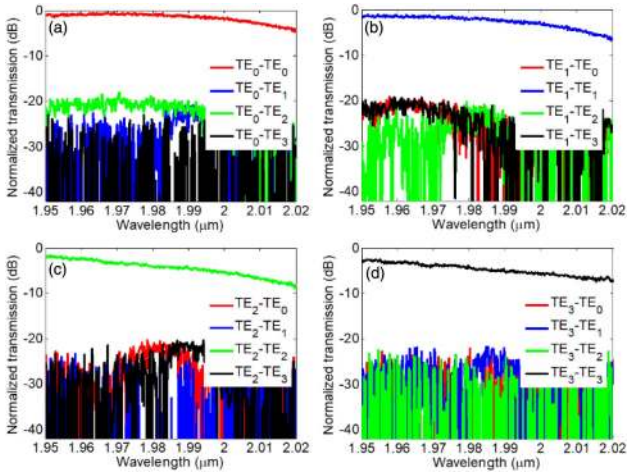

Fig. 5. Measured transmission spectra at four output ports when the TE_0 mode is launched at input ports of (a) CH_1, (b) CH_2, (c) CH_3, and (d) CH_4, corresponding to the TE_0, TE_1, TE_2, and TE_3 modes, respectively.

fabricated narrow and wide tapers are both relatively larger than the designed values in Table 1, which leads to the shift of the central wavelength. Meanwhile, high-order modes suffer from relatively larger scattering loss due to the sidewall roughness of the fabricated waveguide.

The fabricated chip is further employed for the four-mode division multiplexing application with NRZ-OOK signals at 5 Gbit/s. Figure 6(a) shows the experimental setup. An arbitrary waveform generator (Tektronix AWG 70002) is used to generate a 5 Gbit/s electrical OOK signal, and a 2 μm directly modulated laser (DML, EOT ET-5000) is modulated. Then, the optical signal is amplified by a TDFA (AdValue Photonics AP-AMP-2000) and coupled into the waveguide with a pair of vertical gratings. At the receiver side, after transmitting through the mode (de)multiplexer, the light beam is first filtered by a tunable optical filter (TF). After attenuating by a variable optical attenuator (VOA), the optical signal is amplified by another TDFA before being sent to a 2 μm PD. At last, we obtain the electronic signal from a real-time sampling oscilloscope (Keysight DSA-Z 204A) operating at 80 GS/s with a bandwidth of 20 GHz. Figure 6(b) shows the measured spectra around 2 μm before modulation (red) and after modulation (blue). One can clearly see that the optical spectrum with a 5 Gbit/s NRZ-OOK signal (blue) has a wider bandwidth than an unmodulated optical signal (red), indicating successful signal modulation.

Figure 7 plots the measured BER performance of two-channel and four-channel data transmission as a function of the received optical signal-to-noise ratio (OSNR) (back-to-back, CH_1, CH_2, CH_3, and CH_4). The measured OSNR penalties at a BER of 3.8×10^{-3} [7% forward error correction (FEC) threshold] are less than 2.5 dB for four channels. The measured eye diagrams are also obtained in the experiment. Obviously, the penalties are larger than similar experiments demonstrated at 1550 nm [43], and the transmission rate is also limited by the total insertion loss, including the coupling loss of the grating coupler and the intrinsic transmission loss. Moreover, it can be also observed that the BER performance of higher-order modes is not as good as that of the fundamental mode.

Remarkably, the loss of the grating coupler could be reduced by optimizing the etching depth, increasing the thickness of

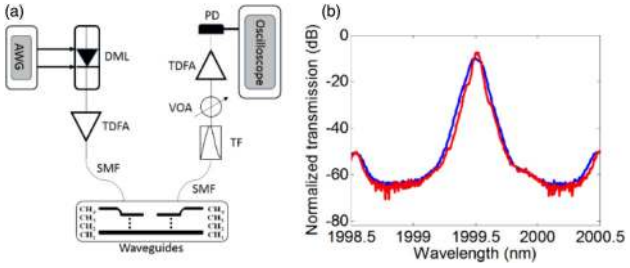

Fig. 6. (a) Experimental setup for 5 Gbit/s OOK data transmission through the MDM system. AWG, arbitrary waveform generator; DML, directly modulated laser; TDFA, thulium-doped fiber amplifier; SMF, single-mode fiber; TF, tunable filter; VOA, variable optical attenuator; PD, photodetector. (b) Measured optical spectra before modulation (red) and after modulation (blue).

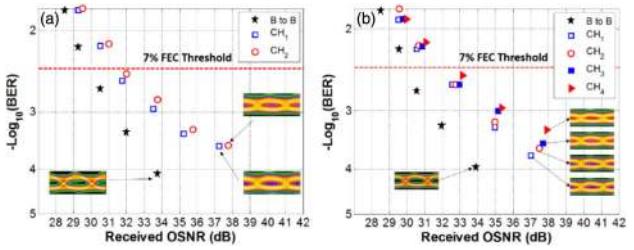

Fig. 7. Measured BER curves versus received OSNR and eye diagrams for (a) two-channel and (b) four-channel data transmission through MDM system. B to B, back-to-back.

silicon, and introducing a complex apodized period. In addition, instead of vertical coupling, the coupling efficiency could be enhanced by edge coupling via inverse tapers.

Moreover, in the present device design, a wide tapered waveguide with $\Delta w = w_{2b} - w_{2a} = 0.1$ μm and a narrow waveguide with width $w_1 = 0.65$ μm are chosen. With further improvement, the narrow and wide silicon waveguides might be both tapered structures with larger Δw (e.g., 0.2 μm) and longer adiabatic coupling length L. Consequently, larger fabrication tolerance and wider working bandwidth could be achieved [46,47].

Additionally, we also study the temperature dependence of the device. The simulated results show favorable operation performance (negligible crosstalk degradation) at different temperatures.

Although the 2 μm communication system can now be implemented by using the components mentioned above, its transmission performance is still limited by the immature 2 μm optoelectronic components. In the experiment, the optical signal at 2 μm is amplified by a TDFA. However, the additional noise introduced by the TDFAs is large, which greatly degrades the transmission performance. In addition, the used TF is not very stable, and its bandwidth is large, which is not efficient for noise suppression. With further improvement of the TDFA (e.g., low-noise TDFA) and TF (e.g., stable and narrow band filter), higher transmission speed up to tens of Gbit/s could be achieved in the experiment.

5. CONCLUSION

In summary, we have fabricated on-chip two-mode and four-mode MDMs and demonstrated on-chip high-speed data transmission in the 2 μm wavelength region. In the experiment, low crosstalks (less than −18 dB) and low insertion losses of all the channels can be obtained. Moreover, chip-scale 5 Gbit/s OOK signal transmission around the wavelength of 2 μm has also been realized. The measured OSNR penalties at a BER of 3.8×10^{-3} are less than 2.5 dB for four channels, and clear eye diagrams are also obtained. In the experiment, the transmission of the 2 μm waveband is still limited by a variety of key optoelectronic devices, such as a modulator, TDFA, filter, and PD. It is believed that the performance including data transmission rate, BER, and transmission distance can be further enhanced by optimizing these essential optoelectronic devices. It is anticipated that the on-chip 2 μm data transmission through the

WDM and MDM will play a key role in emerging MIR spectral applications such as on-chip optical interconnects and on-chip optical data processing.

Funding. National Natural Science Foundation of China (NSFC) (61761130082, 11574001, 11774116, 61705072); Royal Society-Newton Advanced Fellowship; National Program for Support of Top-notch Young Professionals; Natural Science Foundation of Hubei Province (2018CFA048, ZRMS2017000413); Beijing University of Posts and Telecommunications (BUPT)) (IPOC2018A002); Program for HUST Academic Frontier Youth Team (2016QYTD05); Fundamental Research Funds for the Central Universities (2019kfyRCPY037).

Acknowledgment. The authors thank the Center of Micro-Fabrication and Characterization (CMFC) of WNLO and the facility support of the Center for nanoscale characterization and devices of WNLO.

†These authors contributed equally to this work.

REFERENCES

1. R. Soref, "Mid-infrared photonics in silicon and germanium," Nat. Photonics **4**, 495–497 (2010).
2. R. Shankar and M. Lončar, "Silicon photonic devices for mid-infrared applications," Nanophotonics **3**, 329–341 (2014).
3. V. M. Lavchiev and B. Jakoby, "Photonics in the mid-infrared: challenges in single-chip integration and absorption sensing," IEEE J. Sel. Top. Quantum Electron. **23**, 452–463 (2017).
4. M. N. Petrovich, F. Poletti, J. P. Wooler, A. M. Heidt, N. K. Baddela, Z. Li, D. R. Gray, R. Slavík, F. Parmigiani, N. V. Wheeler, J. R. Hayes, E. Numkam, L. Grüner-Nielsen, B. Pálsdóttir, R. Phelan, B. Kelly, J. O'Carroll, M. Becker, N. MacSuibhne, J. Zhao, F. C. Garcia Gunning, A. D. Ellis, P. Petropoulos, S. U. Alam, and D. J. Richardson, "Demonstration of amplified data transmission at 2 μm in a low-loss wide bandwidth hollow core photonic bandgap fiber," Opt. Express **21**, 28559–28569 (2013).
5. Z. Li, A. M. Heidt, J. M. O. Daniel, Y. Jung, S. U. Alam, and D. J. Richardson, "Thulium-doped fiber amplifier for optical communications at 2 μm," Opt. Express **21**, 9289–9297 (2013).
6. H. Zhang, N. Kavanagh, Z. Li, J. Zhao, N. Ye, Y. Chen, N. V. Wheeler, J. P. Wooler, J. R. Hayes, S. R. Sandoghchi, F. Poletti, M. N. Petrovich, S. U. Alam, R. Phelan, J. O'Carroll, B. Kelly, L. Grüner-Nielsen, D. J. Richardson, B. Corbett, and F. C. Garcia Gunning, "100 Gbit/s WDM transmission at 2 μm: transmission studies in both low-loss hollow core photonic bandgap fiber and solid core fiber," Opt. Express **23**, 4946–4951 (2015).
7. M. U. Sadiq, H. Zhang, J. O'Callaghan, B. Roycroft, N. Kavanagh, K. Thomas, A. Gocalinska, Y. Chen, T. Bradley, J. R. Hayes, Z. Li, S.-U. Alam, F. Poletti, M. N. Petrovich, D. J. Richardson, E. Pelucchi, P. O'Brien, F. H. Peters, F. Gunning, and B. Corbett, "40 Gb/s WDM transmission over 1.15-km HC-PBGF using an InP-based Mach–Zehnder modulator at 2 μm," J. Lightwave Technol. **34**, 1706–1711 (2016).
8. K. Xu, Q. Wu, Y. Xie, M. Tang, S. Fu, and D. Liu, "High speed single-wavelength modulation and transmission at 2 μm under bandwidth-constrained condition," Opt. Express **25**, 4528–4534 (2017).
9. W. Bogaerts, R. Baets, P. Dumon, V. Wiaux, S. Beckx, D. Taillaert, B. Luyssaert, J. V. Campenhout, P. Bienstman, and D. V. Thourhout, "Nanophotonic waveguides in silicon-on-insulator fabricated with CMOS technology," J. Lightwave Technol. **23**, 401–412 (2005).
10. R. A. Soref, "The past, present, and future of silicon photonics," IEEE J. Sel. Top. Quantum Electron. **12**, 1678–1687 (2006).
11. R. A. Soref, S. J. Emelett, and W. R. Buchwald, "Silicon waveguided components for the long-wave infrared region," J. Opt. A **8**, 840–848 (2006).
12. J. Wang, "Chip-scale optical interconnects and optical data processing using silicon photonic devices," Photon. Netw. Commun. **31**, 353–372 (2016).
13. J. Wang and Y. Long, "On-chip silicon photonic signaling and processing: a review," Sci. Bull. **63**, 1267–1310 (2018).
14. B. G. Lee, X. Chen, A. Biberman, X. Liu, I.-W. Hsieh, C.-Y. Chou, J. I. Dadap, F. Xia, W. M. J. Green, L. Sekaric, Y. A. Vlasov, R. M. Osgood, and K. Bergman, "Ultrahigh-bandwidth silicon photonic nanowire waveguides for on-chip networks," IEEE Photon. Technol. Lett. **20**, 398–400 (2008).
15. C. Gui, C. Li, Q. Yang, and J. Wang, "Demonstration of terabit-scale data transmission in silicon vertical slot waveguides," Opt. Express **23**, 9736–9745 (2015).
16. J. Du and J. Wang, "Design and fabrication of hybrid SPP waveguides for ultrahigh-bandwidth low-penalty terabit-scale data transmission," Opt. Express **25**, 30124–30134 (2017).
17. Z. Ruan, L. Shen, S. Zheng, A. Wang, Y. Long, N. Zhou, and J. Wang, "Subwavelength grating slot (SWGS) waveguide at 2 μm for chip-scale data transmisson," Nanophotonics **7**, 865–871 (2018).
18. Z. Li, S. U. Alam, Y. Jung, A. M. Heidt, and D. J. Richardson, "All-fiber, ultra-wideband tunable laser at 2 μm," Opt. Lett. **38**, 4739–4742 (2013).
19. J. Li, Z. Sun, H. Luo, Z. Yan, K. Zhou, Y. Liu, and L. Zhang, "Wide wavelength selectable all-fiber thulium doped fiber laser between 1925 nm and 2200 nm," Opt. Express **22**, 5387–5399 (2014).
20. K. Yin, B. Zhang, G. Xue, L. Li, and J. Hou, "High-power all-fiber wavelength-tunable thulium doped fiber laser at 2 μm," Opt. Express **22**, 19947–19952 (2014).
21. S. Latkowski, A. Hänsel, P. J. van Veldhoven, D. D'Agostino, H. Rabbani-Haghighi, B. Docter, N. Bhattacharya, P. J. A. Thijs, H. P. M. M. Ambrosius, M. K. Smit, and K. A. Williams, "Monolithically integrated widely tunable laser source operating at 2 μm," Optica **3**, 1412–1417 (2016).
22. M. A. V. Camp, S. Assefa, D. M. Gill, T. Barwicz, S. M. Shank, P. M. Rice, T. Topuria, and W. M. J. Green, "Demonstration of electrooptic modulation at 2165 nm using a silicon Mach–Zehnder interferometer," Opt. Express **20**, 28009–28016 (2012).
23. J. Chiles and S. Fathpour, "Mid-infrared integrated waveguide modulators based on silicon-on-lithium-niobate photonics," Optica **1**, 350–355 (2014).
24. S. Liu, K. Xu, Q. Song, Z. Cheng, and H. K. Tsang, "Design of mid-infrared electro-optic modulators based on aluminum nitride waveguides," J. Lightwave Technol. **34**, 3837–3842 (2016).
25. W. Cao, D. Hagan, D. J. Thomson, M. Nedeljkovic, C. G. Littlejohns, A. Knights, S. Alam, J. A. Wang, F. Gardes, W. Zhang, S. Liu, K. Li, M. S. Rouifed, G. Xin, W. Wang, H. Wang, G. T. Reed, and G. Z. Mashanovich, "High-speed silicon modulators for the 2 μm wavelength band," Optica **5**, 1055–1062 (2018).
26. J. Wang, J. Hu, P. Becla, A. M. Agarwal, and L. C. Kimerling, "Resonant-cavity-enhanced mid-infrared photodetector on a silicon platform," Opt. Express **18**, 12890–12896 (2010).
27. A. Gassenq, F. Gencarelli, J. Van Campenhout, Y. Shimura, R. Loo, G. Narcy, B. Vincent, and G. Roelkens, "GeSn/Ge heterostructure short-wave infrared photodetectors on silicon," Opt. Express **20**, 27297–27303 (2012).
28. H. Cong, C. Xue, J. Zheng, F. Yang, K. Yu, Z. Liu, X. Zhang, B. Cheng, and Q. Wang, "Silicon based GeSn p-i-n photodetector for SWIR detection," IEEE Photon. J. **8**, 6804706 (2016).
29. J. Wu, Q. Jiang, S. Chen, M. Tang, Y. I. Mazur, Y. Maidaniuk, M. Benamara, M. P. Semtsiv, W. T. Masselink, K. A. Sablon, G. J. Salamo, and H. Liu, "Monolithically integrated InAs/GaAs quantum dot mid-infrared photodetectors on Si substrates," ACS Photon. **3**, 749–753 (2016).
30. N. Hattasan, B. Kuyken, F. Leo, E. M. P. Ryckeboer, D. Vermeulen, and G. Roelkens, "High-efficiency SOI fiber-to-chip grating couplers and low-loss waveguides for the short-wave infrared," IEEE Photon. Technol. Lett. **24**, 1536–1538 (2012).

31. Y. Wei, G. Li, Y. Hao, Y. Li, J. Yang, M. Wang, and X. Jiang, "Long-wave infrared 1 × 2 MMI based on air-gap beneath silicon rib waveguides," Opt. Express **19**, 15803–15809 (2011).
32. M.-S. Rouifed, C. G. Littlejohns, G. X. Tina, Q. Haodong, T. Hu, Z. Zhang, C. Liu, G. T. Reed, and H. Wang, "Low loss SOI waveguides and MMIs at the MIR wavelength of 2 μm," IEEE Photon. Technol. Lett. **28**, 2827–2829 (2016).
33. M. Nedeljkovic, A. Z. Khokhar, Y. Hu, X. Chen, J. Soler Penades, S. Stankovic, H. M. H. Chong, D. J. Thomson, F. Y. Gardes, G. T. Reed, and G. Z. Mashanovich, "Silicon photonic devices and platforms for the mid-infrared," Opt. Mater. Express **3**, 1205–1214 (2013).
34. M. Muneeb, X. Chen, P. Verheyen, G. Lepage, S. Pathak, E. Ryckeboer, A. Malik, B. Kuyken, M. Nedeljkovic, J. V. Campenhout, G. Z. Mashanovich, and G. Roelkens, "Demonstration of silicon-on-insulator mid-infrared spectrometers operating at 3.8 μm," Opt. Express **21**, 11659–11669 (2013).
35. A. Malik, M. Muneeb, Y. Shimura, J. V. Campenhout, R. Loo, and G. Roelkens, "Germanium-on-silicon planar concave grating wavelength (de)multiplexers in the mid-infrared," Appl. Phys. Lett. **103**, 161119 (2013).
36. P. Barritault, M. Brun, P. Labeye, J.-M. Hartmann, F. Boulila, M. Carras, and S. Nicoletti, "Design, fabrication and characterization of an AWG at 4.5 μm," Opt. Express **23**, 26168–26181 (2015).
37. H. Zhang, M. Gleeson, N. Ye, N. Pavarelli, X. Ouyang, J. Zhao, N. Kavanagh, C. Robert, H. Yang, P. E. Morrissey, K. Thomas, A. Gocalinska, Y. Chen, T. Bradley, J. P. Wooler, J. R. Hayes, E. Numkam Fokoua, Z. Li, S. U. Alam, F. Poletti, M. N. Petrovich, D. J. Richardson, B. Kelly, J. O'Carroll, R. Phelan, E. Pelucchi, P. O'Brien, F. Peters, B. Corbett, and F. Gunning, "Dense WDM transmission at 2 μm enabled by an arrayed waveguide grating," Opt. Lett. **40**, 3308–3311 (2015).
38. E. J. Stanton, N. Volet, and J. E. Bowers, "Silicon arrayed waveguide gratings at 2.0 μm wavelength characterized with an on-chip resonator," Opt. Lett. **43**, 1135–1138 (2018).
39. M. M. Milosević, M. Nedeljkovic, T. M. B. Masaud, E. Jaberansary, H. M. H. Chong, N. G. Emerson, G. T. Reed, and G. Z. Ashanovich, "Silicon waveguides and devices for the mid-infrared," Appl. Phys. Lett. **101**, 121105 (2012).
40. B. Troia, A. Z. Khokhar, M. Nedeljkovic, J. S. Penades, V. M. N. Passaro, and G. Z. Mashanovich, "Cascade-coupled racetrack resonators based on the Vernier effect in the mid-infrared," Opt. Express **22**, 23990–24003 (2014).
41. T. Hu, M. S. Rouifed, H. Qiu, X. Guo, C. G. Littlejohns, C. Liu, and H. Wang, "A polarization splitter and rotator based on a partially etched grating-assisted coupler," IEEE Photon. Technol. Lett. **28**, 911–914 (2016).
42. M. Huang, S. Zheng, Y. Long, L. Wang, Z. Ruan, S. Li, L. Shen, and J. Wang, "Experimental demonstration of 2-μm on-chip two-mode division multiplexing using tapered directional coupler-based mode (de)multiplexer," in *Optical Fiber Communication Conference* (2018), paper Tu3A.6.
43. Y. Ding, J. Xu, F. Da Ros, B. Huang, H. Ou, and C. Peucheret, "On-chip two-mode division multiplexing using tapered directional coupler-based mode multiplexer and demultiplexer," Opt. Express **21**, 10376–10382 (2013).
44. J. Wang, S. He, and D. Dai, "On-chip silicon 8-channel hybrid (de)multiplexer enabling simultaneous mode- and polarization-division-multiplexing," Laser Photon. Rev. **8**, L18–L22 (2014).
45. C. Gui, Y. Gao, Z. Zhang, and J. Wang, "On-chip silicon two-mode (de)multiplexer for OFDM/OQAM data transmission based on grating-assisted coupler," IEEE Photon. J. **7**, 7905807 (2015).
46. D. Dai, C. Li, S. Wang, H. Wu, Y. Shi, Z. Wu, S. Gao, T. Dai, H. Yu, and H. K. Tsang, "10-channel mode (de)multiplexer with dual polarizations," Laser Photon. Rev. **12**, 1700109 (2018).
47. J. Wang, Y. Xuan, M. Qi, L. Liu, and G. N. Liu, "Ultra-broadband integrated four-channel mode-division-multiplexing based on tapered mode-evolution couplers," in *European Conference on Optical Communication (ECOC)* (IEEE, 2016), pp. 1–3.